



Effect of Precursor Concentration on the Structural, Optical, and Electrical Properties of WO₃ Thin Films Prepared by Spray Pyrolysis

¹Farhan A. Mohammed, ²Evan T. Salim*, ²Azhar I. Hassan*, ³Mohammed H. A. Wahid

¹Ministry of Industry and Minerals – Iraq

²Department of Applied Sciences, University of Technology – Iraq

³Semiconductor Photonics & Integrated Lightwave Systems (SPILS), School of Microelectronic Engineering, University Malaysia Perlis – Malaysia

Article information

Article history:

Received: February, 15, 2022

Accepted: July, 22, 2022

Available online: December, 10, 2022

Keywords:

Polycrystalline structure,
Thin films,
Tungsten oxide

*Corresponding Author:

Evan T. Salim

evan.t.salim@uotechnology.edu.iq

Abstract

Using a chemical spray technique, an n-type WO₃ polycrystalline thin film was prepared with optimizing parameters (molarity concentration of 80 mM and a substrate temperature of 350 °C). Study the physical properties of WO₃ thin film via UV-Visible spectroscopy, XRD, Field Emission-Scanning Electron Microscope, Energy Dispersive X-ray Spectroscopy, Atomic Force Microscopy, and current-voltage. Tungsten oxide was deposited on glass surfaces at different molarities ranging from 50–90mM. In the UV-Visible spectrum of the WO₃ thin film, it was found that the transmittance, reflectivity, and energy gap decreased (78%–53%), (9.63%–5.02%), and (3.40eV–2.63 eV), respectively. The X-ray diffraction of the WO₃ film at the optimized was poly-crystalline and had a monoclinic phase, and the preferred orientation (hkl) was 200 at $2\theta = 24.19$. From the image FESEM and EDX, it was found that it has a multi-fibrous network. The average diameter of the fiber is 266 nm, and the ratio of tungsten to oxygen (W/O) is 2.6, with a stoichiometric of 68.6% at the 80 mM concentration. The Atomic Force Microscopy shows that the WO₃ thin layer has a nanostructure. The average surface roughness was 5.3 nm, and the Root Mean Square was 8.6 nm. The WO₃ film had the lowest resistivity value of $2.393 \times 10^8 \Omega \text{ cm}$, and the activation energy was 0.298 eV, among the parameter of the current voltage at substrate temperature and concentration optimum.

DOI: [10.53293/jasn.2022.4715.1139](https://doi.org/10.53293/jasn.2022.4715.1139), Department of Applied Sciences, University of Technology

This is an open access article under the CC BY 4.0 License.

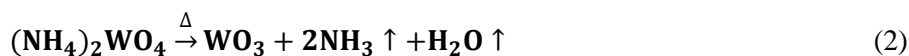
1. Introduction

Because of its high operational stability, broadband gap, charge carrier recombination ability, and environmental durability, transition metal oxide (TMO) is now the most appealing choice for deployment in the microelectronic device sector [1-4]. Tungsten trioxide (WO₃) is a multi-functional material with several unique features,

including sharp phase transitions, higher UV–Vis light absorption, high crystallinity, and effective surface structures. WO_3 is a significant component of an n-type semiconductor that has been extensively explored in thin-film form for advanced technological applications. WO_3 films come in a variety of polymorphs depending on the preparation method: monoclinic ($\gamma\text{-WO}_3$), orthorhombic ($\beta\text{-WO}_3$), tetragonal ($\alpha\text{-WO}_3$), triclinic ($\delta\text{-WO}_3$), and hexagonal (h-WO_3). The optical, electrical, and sensing characteristics of all these phases are excellent [5]. The recent finding of potential uses in organic light-emitting diodes has revived interest in tungsten oxide WO_3 thin films [6]. It has organic photovoltaic devices [7], super hydrophilic [8], photocatalysis [9], electrochromic devices [10], gaschromic [11], photocatalytic [12], and photoluminescence (PL) properties [13]. It can be used in fuel cell applications [14], gas sensors [15], and other applications. Because of its large surface-to-volume ratio, WO_3 can be easily manufactured in a thin film to create unique physical and chemical properties. There is a large amount of transparency and good transmission capabilities in the visible area. Thin-film WO_3 has already been used in the next generation of products, such as clever windows [16], eyewear, anti-distracting rear view mirrors for cars [17], and electronic noses [4], in addition to non-emitting displays. However, WO_3 nanoparticles have been intelligently engineered and produced in various forms. Based on the flaws listed above, WO_3 nanoparticles with high dispersity and ultra-small diameters could increase the performance of nanoparticle-based sensors. Li et al. [18]. Produced highly dispersible WO_3 nanoparticles with diameters ranging from 10 to 50 nm and discovered that the constructed sensor performed well. Due to the extremely sensitive sensors, it demonstrated exceptional gas sensing capabilities. Adequate vacancy and efficient surface area. V.V. Ganbavle et al. [19]. Present their findings in this paper. The effect of solution concentration on the structural, optical, morphological, and electrical properties of the tungsten oxide film is studied. It was found that the films were polycrystalline and monoclinic in phase, which was similar to our research results. S. S. Shendage [20]. Furthermore, the synthesis of a porous fibrous network of WO_3 thin films was found in the study to have an energy gap and activation energy greater than the values obtained in our work. In another study, P. T. K. Shanimugasudram et al [21]. The effect of concentration on the structural properties was observed by increasing the intensity of the peaks and increasing the electrical conductivity at optimum conditions. There was an improvement in our results. L. Sunasri et al [22]. They evaluated tungsten trioxide films where increased concentration increased thickness, consistent with our results. R.M. et al. [4] detailed evaluation of WO_3 -nanoplate can decrease the energy gap of the film, but the value obtained was much greater than our value. A variety of techniques have been used to create WO_3 thin films, including thermal evaporation [23], laser deposition [24], Radio-frequency sputtering [25], Electron beam deposition or evaporation [26], Anodic oxidation [27], sol-gel [28], hydrothermal [29, 30], spray pyrolysis [31], as well as others. In this study, the spray pyrolysis technique was used for the preparation of the film because it is an easy, effective, and non-vacuum coating approach that enables the creation of huge areas of thin films at a low cost. Electronic and optoelectronic applications in various devices require certain precursor conditions. These qualities, such as nanoscale geometry, are significantly controlled by the particle size and form of the nanostructures. Hence, any technological application requires rigorous characterization, measurement, and knowledge of numerous physical parameters. Furthermore, the films exhibit varying nanostructure properties like grain size, grain boundary, the roughness of the surface, and so on, depending on the various methods and processing factors used, which affect the films' optical and electrical behaviour.

2. Experimental Procedure

Tungsten oxide thin films were prepared using tungsten acid H_2WO_4 (Merck- Germany) powder by chemical spraying technique on glass substrates with dimensions of $2 \times 2 \text{ cm}^2$. Further, 50mM, 60mM, 70mM, 80mM, and 90mM of tungsten acid powder were dissolved in 50 ml of ammonium hydroxide solution (NH_4OH) (Belgium) at 80°C on a hot plate with a magnetic sterile for 10 min until the form of the solution was clear as shown in the chemical reaction below [32].



Ammonium tungstate ($(\text{NH}_4)_2\text{WO}_4$) was sprayed on glass substrates at 350°C to form tungsten oxide films. The distance between the spray nozzles and the substrates was fixed at 28.5 cm, and the compressed air was 1.72 bar

at a spray rate of 3 ml/min. The formation of tungsten oxide films is shown in the above chemical equation [32]. The optical characterization was obtained using UV-Visible spectroscopy (UV-1800, SHIMADZU) and Diffused Reflectance UV-VIS Spectrometer (Avalight-DH-S-BAL). The structural properties of tungsten oxide were analyzed using X-ray diffraction (SHIMADZU-6000, Japan) with wavelength 1.54060 Å (CuKα1). A surface morphology study was carried out using Field Emission Scanning Electron Microscope FESEM (Zeiss Sigma). Atomic force Microscopy (AFM-AA 3000 USA) was used to analyze the surface roughness of the WO₃ thin film. The electrical conductivity of the WO₃ film was calculated using the Keithley source meter (model no.2400 USA).

3. Results and Discussion

3.1. UV-Visible Properties

A UV-Visible spectrometer with a wavelength range of 250–1100 nm and a UV-Vis diffuse reflectance spectrometer were used to evaluate the optical characteristics of the WO₃ thin films. Figure 1a shows the optical transmittance spectra of WO₃ thin films sprayed on quartz substrate at different concentrations (a). The transmission spectrum of WO₃ films demonstrates that when the precursor concentration (50–80) mM increases, the transmission decreases. Later, at 90 mM, it climbed little (78%, 77%, 65%, 53%, and 62%), respectively, were the highest transmission rates. Because there were more W ions in the greater precursor molarity, the transmission reduced, resulting in a thicker layer [33, 46, 47]. We saw an increase in transmission when the solution concentration was increased to 90 mM. This could be due to the film's thickness decreasing and the reduction in light dispersion in grain boundaries [48, 56]. Figure 1b shows the variations in optical absorbance of WO₃ thin film at the various concentrations indicated above; at a wavelength of 250 nm, all the films have a strong absorption.

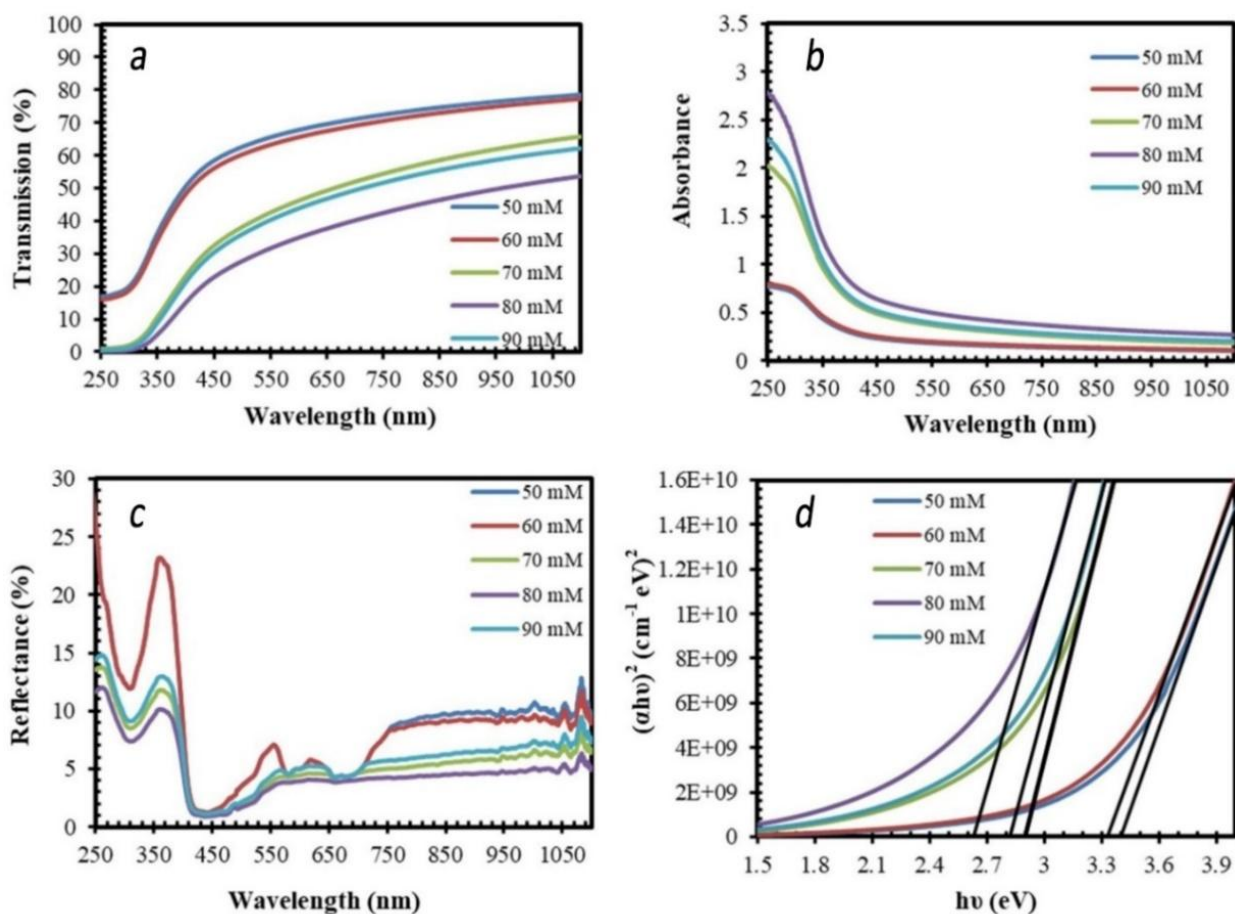


Figure 1: (a) optical transmittance, (b) absorbance, (c) Reflectance, (d) Energy gap of WO₃ thin films at variation molarity concentration.

The absorbance levels then steadily drop to 380 nm before stabilizing at longer wavelengths. While the molar concentration varied from 50 mM to 90mM of WO₃, the optical absorbance of the films decreased up to 70 mM and then increased to 80 mM, which resulted from the increase in thickness of the film and grain boundaries [34]. The decrease in the optical absorbance with increasing the concentration to 90mM indicates a reduction in the thickness of the film. Also, because of the inverse relationship between transmittance and absorbance [35]. The characteristics of reflectance for WO₃ thin films were evaluated by UV-Vis diffuse reflectance spectra (DRS), which show exceptionally low reflectance at wavelengths (380-480) nm, as shown in Figure 1c. By studying the optical and figure of merit of the films at different molar concentrations, it was found that the best concentration is 80mM. Figure 1b illustrates optical absorption for WO₃ thin films formed at different molarity concentrations (50, 60, 70, 80, and 90mM), with each film having a strong absorption at 250 nm and subsequently decreasing towards longer wavelengths [4]. The absorption of WO₃ thin films sprayed at 50–80 mM solution concentrations increased with increasing g solution concentration, then reduced at 90mM. This is because the thickness has increased and decreased [33, 42, 43]. As the solution concentration rises, the thickness of the WO₃ thin films and the number of particles grow [29, 44]. Extrapolation of the linear relationship among $(\alpha h\nu)^2$ and $h\nu$ given in the equation is used to estimate the gap of Energy for WO₃ thin films (8) [37].

$$(\alpha h\nu)^2 = A(h\nu - E_g) \quad (3)$$

The photon energy is $h\nu$, the optical band gap is E_g , and the constant is A. The gap of energy (E_g) values is estimated from the plot of $(\alpha h\nu)^2$ vs. the energy of photon $h\nu$ in Figure 1d, which shows the WO₃ films' direct band gap energy. The energy band is determined by the linear part of the energy axis (E_g). Table 1 shows the expected values for E_g . As the molarity concentration increased to 80 mM, the band gap values of WO₃ thin films decreased from 3.40 to 2.63 eV, then climbed to 2.82 eV, as displayed in Figure 1d, which is in good agreement with research [4, 20, 21]. The decrease in band gap energy was caused by a lattice defect that may create energy tails within the energy gap, shifting the Fermi level towards the conduction band [51]. Additionally, due to the films' increased crystallinity [52]. Additionally, strain fluctuations are responsible for the decreasing band gap. Strain influences the energy gap by altering semiconductors' interatomic spacing. [46]. Our findings matched those of the researchers [4,48]. However, once the molarity concentration was increased to 90mM, the energy band gap rose, and this rise in poor gap energy may be attributed to a decrease in band tail width, which agreed with the study [50]. We estimated the significant optical characteristics such as coefficient of absorption(α), coefficient of extinction(k), optical conductivity(σ_{opt}), and refractive index(n) of the WO₃ thin films via the relationships [53, 54], and the results are shown in Table 1.

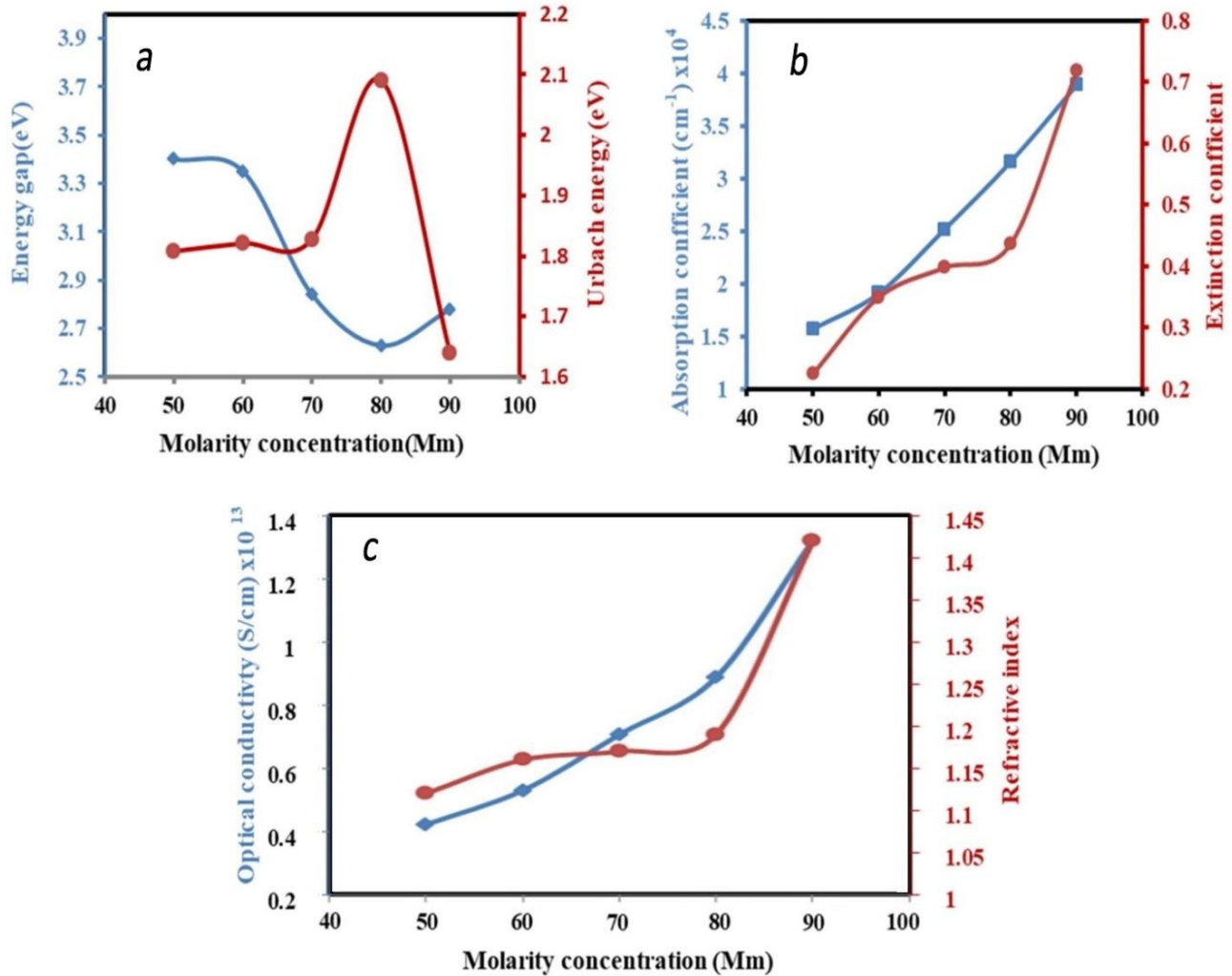
$$\alpha = \frac{\ln \frac{1}{T}}{t} \quad (4)$$

$$k = \frac{\alpha \lambda}{4\pi} \quad (5)$$

$$\sigma_{opt} = \frac{nc\alpha}{4\pi} \quad (6)$$

$$n = \frac{1+R}{1-R} \pm \sqrt{\frac{4R}{(1-R)^2} - K^2} \quad (7)$$

Where α is the absorption coefficient, n is the refractive index, c is the light velocity, R is the reflectance, T is the transmittance, t is the film thickness, and K is the extinction coefficient. The optical characteristics of the



coefficient of absorption, extinction coefficient, optical conductivity, and refractive index of tungsten oxide films were raised with increasing molarity concentration, as displayed in Figure 2a, 2b, and 2c at varying concentrations from 50 mM to 90mM, because of the improved impact of electron transitions between both the two bands (i.e., valance band and conduction band), the calculated σ_{opt} increases with molarity concentration, reducing the energy gap [4]. Due to improved density of packing and layer thickness with a reduced extinction coefficient, the refractive index(n) value improved steadily, increasing molarity concentration [4].

Figure 2: Variation of an optical parameter versus various molarity concentrations, a. Energy gap and Urbach energy, b. absorption coefficient and Extinction coefficient, and c. optical conductivity and Refractive index.

For many materials, the absorption coefficient (α) near the band ledge is thought to have an exponential relationship with photon energy $h\nu$. The relationship derived from Urbach explains this reliance [55].

$$\alpha = \alpha_0 \exp\left(\frac{h\nu}{E_u}\right) \quad (8)$$

E_u denotes the breadth of the tailpiece of the localized states linked with the forbidden gap's amorphous region and is α_0 constant. E_u is determined using a reverse of the slope of the linear component in the lower photon energy zone, and the results are shown in Table 1. The optical band gap energy has an inverse relationship with E_u values. The exponential dependency of the coefficient of absorption near the optical absorption ledge is described using the tail of Urbach (E_u). The disorder causes a change of the Urbach tail (E_u) in the materials,

which leads to an extended parabolic density of states into the band edge. The disorder includes thermal disorder, which reflects the thermal occupation of phonon states, or structural disorder, which is associated with impurities and defects in the material. In this case, the Urbach tail was attributed to the effects of solution concentration on the fundamental optical absorption [56].

Table 1: Optical parameters of WO₃ thin film deposited at various mole concentrations.

Mole concentration(mM)	Av. Absorption coefficient x104 (cm ⁻¹)	Av. Extinction coefficient (k)	Band gap (eV)	Av. Optical conductivity σ_{opt} 1013(Ω cm) ⁻¹	Urbach energy (eV)	Av. Refractive index(n)	Av. thickness (nm)
50	1.5731	0.2244	3.40	0.4218	1.808	1.127	300
60	1.9152	0.3496	3.35	0.5295	1.821	1.162	1000
70	2.5254	0.3979	2.84	0.7071	1.828	1.177	1043
80	3.1662	0.4363	2.63	0.8883	2.091	1.195	1737
90	3.8985	0.7183	2.78	1.3218	1.639	1.425	1250

3.2. X-ray Diffraction (XRD)

The structural alterations and phase of as-synthesized WO₃ thin films are investigated with an X-ray pattern. Figure 3 depicts the XRD diffraction of the WO₃ thin film sample coated on glass substrates at 350°C and 80mM molarity. The XRD peaks were indicated to the monoclinic phase of WO₃, indicating its pristine crystal structure in the absence of secondary or impurity phases (JCPDS Card No.43-1035) [42]. The XRD shape can be seen a well-defined peak triplet, which can be indexed as (002), (020), and (200) at $2\theta = 23.21, 23.68,$ and $24.19,$ respectively, and is attributed to monoclinic WO₃ with a favored (200) plane. Lower intensities of various diffraction peaks have also been recorded at 2θ values of 28.103, 33.917, 41.819, 49.658, 55.669, and 55.517, which correspond to the (hkl) planes (112), (202), (222), (400), (214), and, which corresponds with the study [33]. Higher peak intensity correlates with higher crystallinity, although other investigations have demonstrated that the film thickness can also influence this. We noticed that when the molar concentration increased, the intensity of the peaks increased, especially when (hkl) was (200) [36]. At high concentrations, the film is formed as a powder, which increases the grain size, but the crystallinity of the film decreases because of the incomplete decomposition of the solution [19]. The Debye-Scherrer eq. (3) evaluates the crystallite size of polycrystalline WO₃ films for the strongest peaks. The results obtained from X-ray diffraction agreed with the report [19,20].

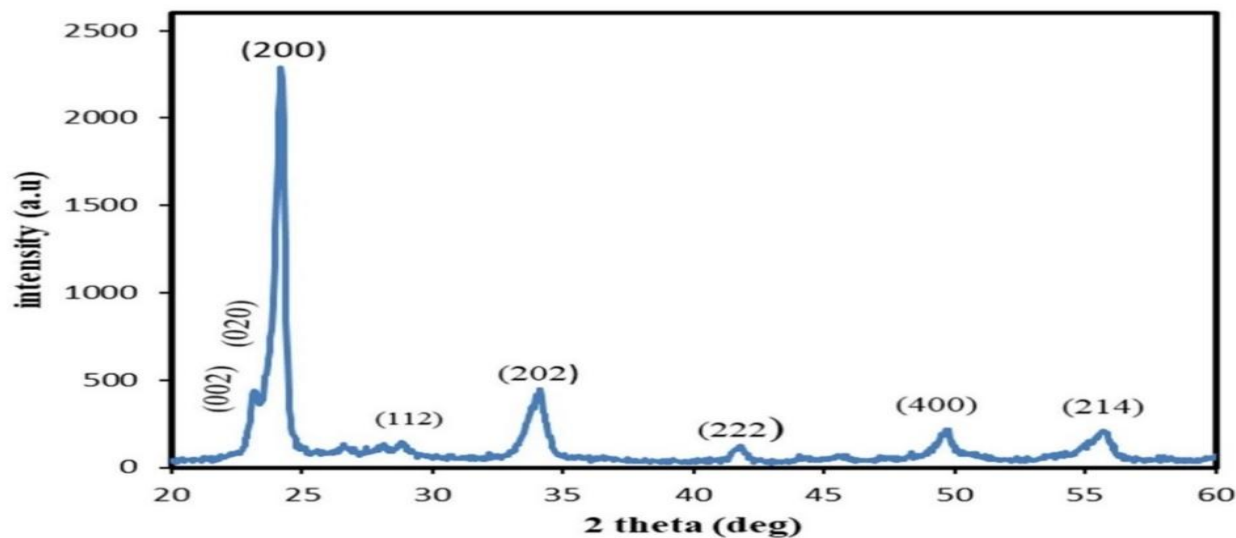


Figure 3: X-ray diffraction shapes of deposited WO₃ thin layer created utilizing spray pyrolysis process at optimal substrate temperature with molarity concentration of 80mM.

$$D = \frac{0.9\lambda}{\beta \cos \theta} \quad (9)$$

Where D is the crystallite size, 1.54056Å is the Cu K α line wavelength, is the whole width at half maximum for the corresponding peak, and Bragg's angle in radian. Table 2 displays the structural properties of WO₃ thin films at an ideal concentration of 80mM. At ideal molarity concentration, the average crystallite size (D_{avg}) for the WO₃ Film improved as the FWHM decreased t. Measurement of the microstrain is a significant parameter in determining the mechanical stability of the films. Equations (10), (11), and (12) were used to determine microstrain(ϵ), the density of dislocation (δ), and stacking fault (SF) [38].

$$\epsilon = \frac{\beta \cos \theta}{4} \quad (10)$$

$$\delta = \frac{1}{D^2} \quad (11)$$

$$SF = \left[\frac{2\pi^2}{45(3\tan\theta)^{1/2}} \right] \beta \quad (12)$$

$$TC = \frac{I_o(h_k l_i)}{I_s(h_k l_i)} / \left[\frac{1}{N} \sum \frac{I_o(h_k l_i)}{I_s(h_k l_i)} \right] \quad (13)$$

Table 2: The structural properties of WO₃ thin films at an optimal concentration of 80mM.

Molarity concentration (mM)	2 θ (°)	hkl	d(Å)	FWHM(β) (rad)	D (nm)	$\delta \times 10^{14}$ lines m ²	$\epsilon \times 10^{-3}$ line ⁻² m ⁻⁴	stacking fault (SF) $\times 10^{-2}$	Texture coefficient
80	23.21	002	3.82848	0.00781	18.15	3.03503	0.19138	0.251	0.9508
	24.19	200	3.67529	0.00760	18.61	2.88496	0.18592	0.240	0.9418
	28.84	112	3.09237	0.00778	18.02	3.07709	0.18838	0.224	0.9314
	33.97	202	2.63617	0.01353	10.23	9.55259	0.32366	0.357	1.0795
	41.73	222	2.16270	0.00999	13.53	5.45558	0.23352	0.236	1.0779
	49.61	400	1.83592	0.01046	12.56	6.33851	0.23754	0.224	1.0182

Microstrain, dislocation density, and stacking fault all decreased with diffraction angle, indicating a reduction in lattice defects at the interplanar spacing of the crystal [39,40]. Table 2 shows the results. One of the basal structural properties of polycrystalline materials is the texture coefficient, Using the formula (13) [41]. Where TC is the (hkl) plane's texture coefficient, I_o (hkl) is the estimated relative intensity, and I_s (hkl) is the corresponding plane's JCPDS standard intensity. N is the number of reflection peaks in general; the coefficient of texture (TC) for a film with a preferred location in any (hkl) plane must be at least 1. As shown in the table, the value of TC of the films made at ideal concentrations equals one (1). This suggests that tungsten oxide coatings develop preferentially [4,39].

3.3. FE-Scanning Electron Microscopy and EDX

The morphology of the thin WO₃ layer in Figure 4a was examined using FESEM. The proper concentration (80mM) was applied to the glass substrate at 350 °C. Furthermore, with an 80mM concentration, the WO₃ thin film has a reticulated fibers structure with an average fiber diameter of 266 nm. This may be supported by a study [36]. The internal fiber network was seen with different fiber diameters for 80mM. This was caused by the impact and decay of tiny droplets on the substrate, with the decay and overlapping of droplets repeatedly

occurring [42]. In addition, pictures of the WO_3 thin film obtained by FESEM reveal a fiber network with an internal fiber network with a diameter of 70 nm. The films appear to be made up of many layers of fibrous material [43]. Scanning electron microscopy was used to visualize a cross-sectional WO_3 thin layer in Figure 4b, 4d, 4e, 4f, and 4g. At 350°C ($1.7\ \mu\text{m}$), the appropriate concentration (80mM) was placed on the glass substrate. The inset in Figure 4b displays the EDX spectrum of a spray-coated WO_3 thin sheet with a mol concentration of 80mM. (c). The estimated elements, tungsten, and oxygen were found in the spectrum without undesirable contaminants. The atomic ratios of (W %, O %), and stoichiometry (%), respectively, were (19.47, 80.53, and 68.6). The amount of oxygen in the WO_3 film can have a significant impact on the electrical conductivity as well as the morphology and structure revealed by the XRD and FESEM results.

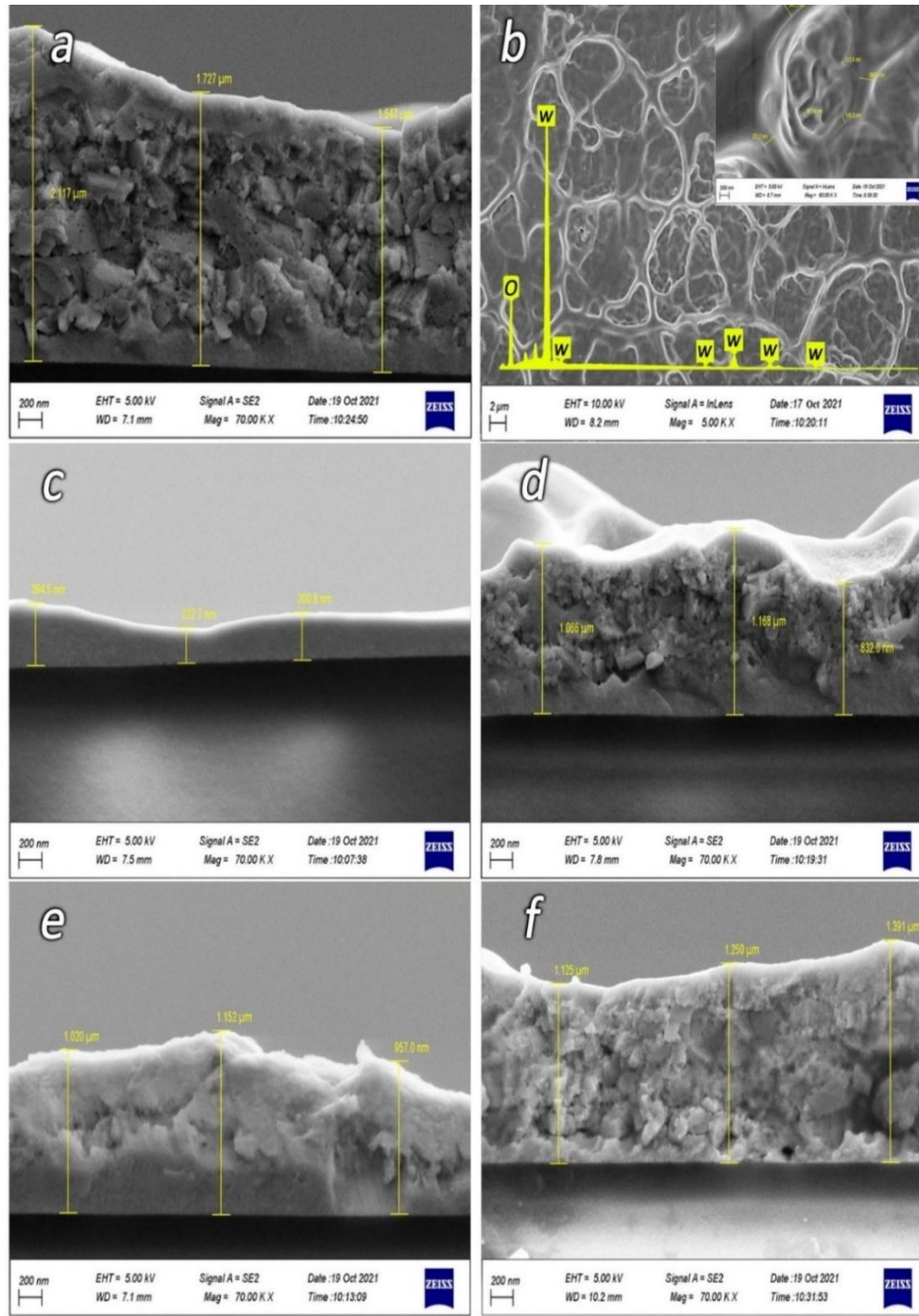


Figure 4: (a) shown FE-SEM, (b, d, e, f, g) cross-section, and (c) EDX of WO_3 thin film at substrate temperature 350°C , and optimal concentration of 80mM

3.4. Atomic Force Microscopy

Figure 5 shows an AFM image of WO_3 thin film with an 80mM molarity concentration. Images from Atomic Force Microscopy (AFM) are captured in a $5\mu\text{m} \times 5\mu\text{m}$ area. The WO_3 films have particle sizes, average roughness, and root means square of (82.63, 5.3, and 6.8) nm, respectively. The layers show a fibrous reticulate-like shape at 80mM, one of metal oxides' features [44]. The improvement of surface morphology and decrease in mean roughness were obtained at optimal concentration, as demonstrated in the above results. A sample with a denser shape and overlaid islands were coated from a precursor solution with greater molarity of 80mM. When aerosol droplets collide with a solid surface, the reactant molecule's potential is lowered, and they may bond to the substrate, resulting in separate nuclei. The interaction of tungsten-containing species with already formed nuclei accelerates the formation of films, which is aided by the continual adsorption of the droplets onto the surface. A sample deposited from a precursor solution with higher molarity (80mM) has a denser morphology with superimposed islands. When the aerosol droplets strike the solid surface, the collision decreases the energy of the reactant molecules, and they may bind to the surface, forming isolated nuclei. Continuous adsorption of the droplets assists the film growth onto the substrate, followed by the reaction between the tungsten-containing species and the already formed nuclei. After monolayer(s) formation on the substrate, island formation occurs, probably because of the decreased binding energy of the chemical species to the existing layers because the concentration of reactants on the surface reaches a saturation point under the chosen experimental condition (island-layer Stranski–Krastonov) mechanisms [45]. We noticed that when the concentration was increased to 80mM, the roughness and Root mean square decreased, which the researcher agreed with [6].

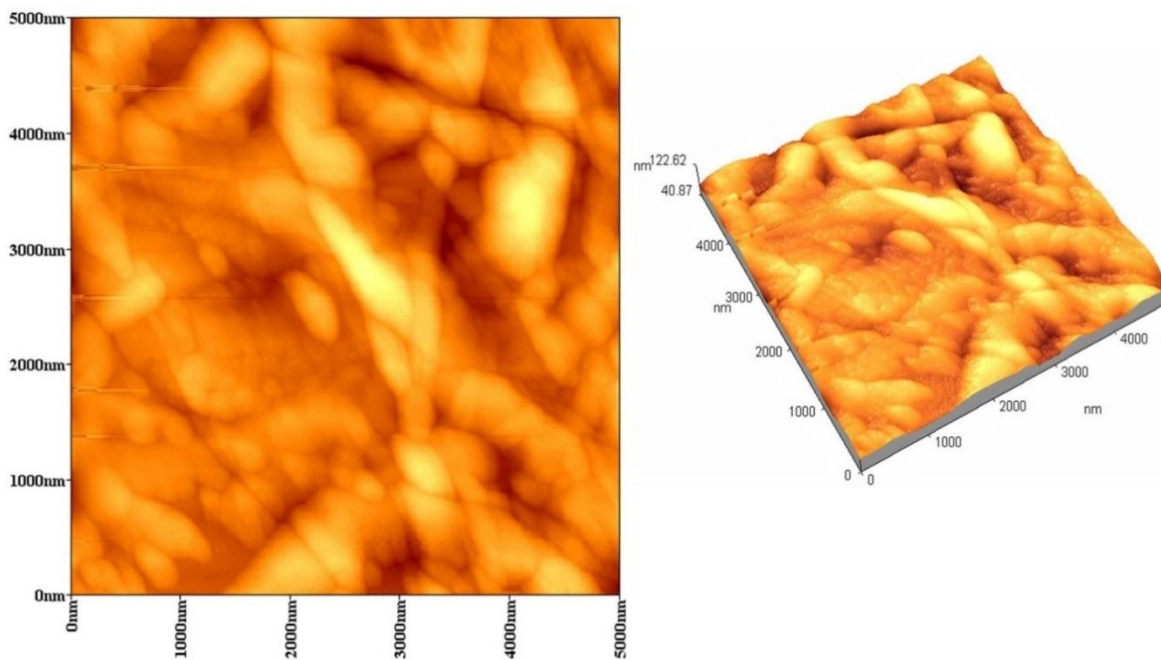


Figure 5: AFM images at an optimal concentration of the WO_3 thin film with substrate temperature 350°C

3.5. Electrical Conductivity

As shown in Figure 6a, at different temperatures (303–423) K, the current-voltage properties of spray-coated WO_3 nanofiber films were investigated, and the measured results of I are shown to grow linearly with applied voltage was (10–100) V at varied measurement temperatures. The I – V characteristics reveal that the corresponding curve grew exponentially when the film's measurement temperature increased. When evaluated at 423K, the film showed more significant progress and a higher I value than when measured at 303K. The opposition was lessening. As a result of the increased heat energy at higher temperatures, electrons may be liberated from the lattice for conduction [42]. The films with the least amount of oxygen in them probably performed better. When compared to other temperatures, I value are exceptionally high at 423K [4]. The electrical DC conductivity was computed using the following equation (14) [21,57].

$$\sigma = \left[\frac{I}{V} \right] \times \left[\frac{d}{A} \right] \quad (14)$$

I denotes the current, V indicates the applied voltage, D is the inter-probe distance, and A is the film's cross-sectional area. The average values of conductivity and resistivity are 4.1762×10^{-8} s/cm and 2.393×10^{-8} Ω .cm, which is in good agreement with the researcher [21,40]. Based on computed conductivity at an optimal solution concentration of deposited WO_3 thin film. Conductivity increased with grain size due to the reduction in grain boundary volume and related impedance to the flow of charge carriers [57]. On the other hand, the increased thickness can improve the thin film's crystalline size, resulting in fewer trapping states at grain boundaries. On the other hand, increased film thickness leads to an increase in carrier concentration [58]. The plot of Arrhenius ($\ln(\sigma)$ vs. $1/T$) for various molarity of WO_3 films is shown in Figure 6b.

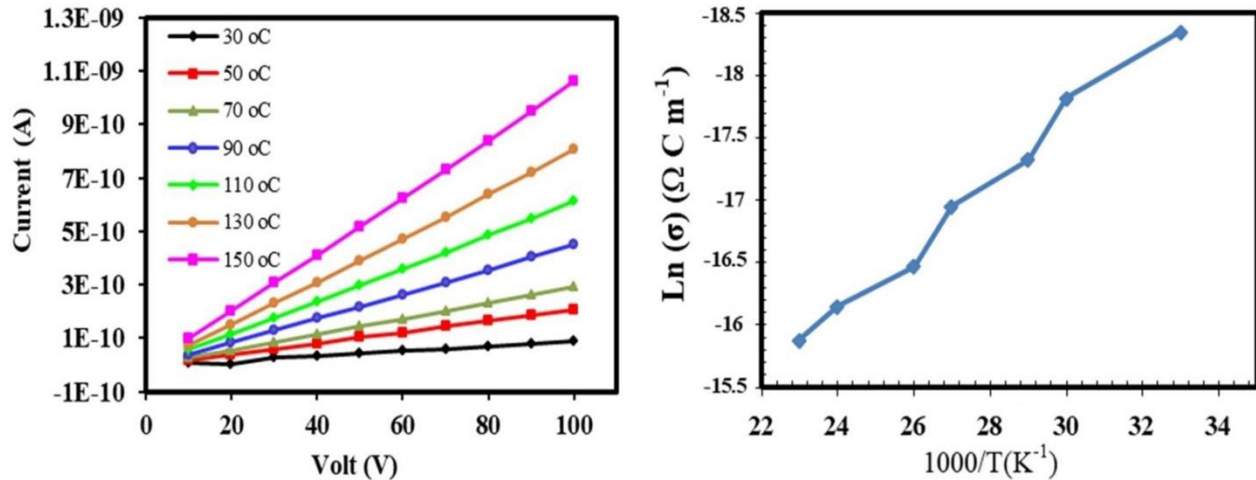


Figure 6: (a) I-V characterization, (b) shows the plot of Arrhenius ($\ln(\sigma)$ vs. $1/T$) of WO_3 thin films at 80 molarity concentration.

The Arrhenius Equation can be used to compute the activation energy (E_a) [57].

$$\sigma = \sigma_0 \exp\left(\frac{-E_a}{K_B T}\right) \quad (15)$$

where σ is the conductivity of electrical, σ_0 represents a constant, E_a is the energy of activation, K_B is the constant of Boltzmann, and T represents the temperature of absolute.

In an 80mM molarity concentration, the activation energy was 0.298 eV. This could be due to stoichiometry, which raises the charge carrier concentration collision [42].

3.5. Figure of Merit

Optimization between the electrical conductivity and optical transparency could be obtained from the value of the figure of merit using equation (16) [60] shown in Figure 7 as a function of the molarity concentration.

$$F.O.M = \frac{1}{\rho \ln T_{Avg}} \quad (16)$$

Where ρ is the resistivity (cm Ω), and T is the average of transmittance. The F.O.M of the produced thin films increased as the molarity increased, as seen in Figure 7. Many variables support this increase, including improvements in structural qualities as measured by x-ray diffraction, topography augmentation, and transmission reduction. This indicates that the molarity concentration of 80mM is the best for achieving the best photodiode properties.

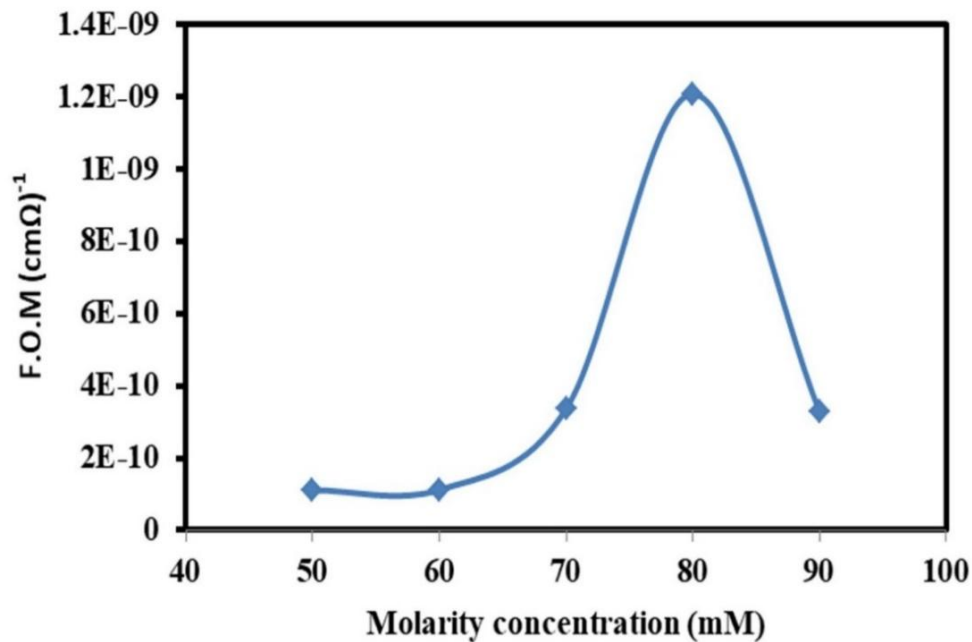


Figure 7: F.O.M as a function of the molarity concentration for WO₃ thin films at substrate temperature 350 °C.

4. Conclusions

The optical transmittance and reflectance of the WO₃ thin films, which were synthesized at 350 °C on glass substrates with an increase in molarity concentration from 50 mM to 80 mM, decreased from 78 percent to 53 percent and from 9.63 percent to 5.02 percent, respectively. The WO₃ thin films, which were formed at 350 °C on glass substrates with an increase in molarity concentration from 50 mM to 80 mM, show a decrease in optical transmittance and reflectance from 78 to 53% and from 9.63 to 5.02%, respectively. The direct energy gap of WO₃ thin films decreased to 2.63 eV, while Urbach energy increased to 2.091 eV at 80mM. From the X-ray diffraction study, the films indicate a polycrystalline structure with a monoclinic phase with the preferred orientation at (hkl) of 200. The average grain size is 18.61 nm under the optimal parameter, while the other peaks were intensely low at (hkl) of (002), (112), (202), (222), (400), and (214). From the image of the field emission scanning electron microscope, it was found that it possesses a fibrous network with an average diameter of 266 nm. The thickness of the sample is 1700 nm in cross-sectional measurement. The EDX spectra of the WO₃ film produced at optimized parameters (80mM) showed that the atomic ratios of (W %, O %) were (19.47 and 80.53) respectively. The average roughness and root mean square of the tungsten oxide thin film were around 5.3nm and 6.8nm, respectively. To evaluate the electrical properties of the WO₃ film deposited at a molar concentration of 80mM, the highest conductivity (4.1762x10⁻⁸ s/cm), and the activation energy (0.298 eV). These results, which included the optical, structural, and electrical properties of WO₃ thin films, make them very suitable for optoelectronic devices.

Conflict of Interest

The authors declare that they have no conflict of interest.

References

- [1] L. G. Gerling, S. Mahato, C. Voz, R. Alcubilla, J. Puigdollers, et, al., "Characterization of transition metal oxide/silicon heterojunctions for solar cell applications," *Applied sciences*, vol. 5, no. 4, pp. 695-705, 2015.
- [2] A. A. Al-Ghamdi, H. Bostancı, O. A. Al-Hartomy, M. Soyulu et. al., "Preparation of tungsten trioxide nanorods by hydrothermal route: n-tungsten trioxide nanorods/p-silicon p-n junction," *Journal of Nanoelectronics and Optoelectronics*, vol. 9, no. 3, pp. 327-333, 2014.

- [3] J. C. M. Raja, M. Balaji, and P. Kathirvel, "Investigation of microstructural and optical and dc electrical properties of spin coated Al: WO₃ thin films for n-Al: WO₃ / p-Si heterojunction diodes" *Optik*, vol. 145, pp. 169-180, 2017.
- [4] R. M. J. C. S. M. P. V. V. B. P. Balraju³, "Jet Nebulizer Sprayed WO₃ Nanoplate Arrays for High Photoresponsivity Based Metal-Insulator-Semiconductor Structured Schottky Barrier Diodes," *Journal of Inorganic and Organometallic Polymers and Materials*, 2019.
- [5] A. Faudoa-Arzate, A. Arteaga-Durán, R. Saenz-Hernández, M. Botello-Zubiate, P. Realyvazquez-Guevara, and J. Matutes-Aquino, "HRTEM microstructural characterization of β -WO₃ thin films deposited by reactive RF magnetron sputtering," *Materials*, vol. 10, no. 2, pp. 200, 2017.
- [6] Z. Hai, Z. Wei, C. Xue, H. Xu, and F. Verpoort, "Nanostructured tungsten oxide thin film devices: from optoelectronics and ionics to iontronics," *Journal of Materials Chemistry C*, vol. 7, no. 42, pp. 12968-12990, 2019.
- [7] S. Kim, M. A. Saeed, S. H. Kim, and J. W. Shim, "Enhanced hole selecting behavior of WO₃ interlayers for efficient indoor organic photovoltaic with high fill-factor," *Applied Surface Science*, vol. 527, pp. 146840, 2020.
- [8] N. D. Quang, P. C. Van, S. Majumder, J.-R. Jeong, D. Kim, and C. Kim, "Optimization of photogenerated charge transport using type-II heterojunction structure of CoP/BiVO₄: WO₃ for high efficient solar-driver water splitting," *Journal of Alloys and Compounds*, vol. 899, pp. 163292, 2022.
- [9] P. Uppachai, V. Harnchana, S. Pimanpang, V. Amornkitbamrung, et, al., "A substoichiometric tungsten oxide catalyst provides a sustainable and efficient counter electrode for dye-sensitized solar cells," *Electrochimica Acta*, vol. 145, pp. 27-33, 2014.
- [10] Y. Zhen, B. P. Jelle, and T. Gao, "Electrochromic properties of WO₃ thin films: The role of film thickness," *Analytical Science Advances*, vol. 1, no. 2, pp. 124-131, 2020.
- [11] S. Xue, G. Gao, Z. Zhang, X. Jiang, J. Shen, G. Wu, H. Dai, Y. Xu, and Y. Xiao, "Nanoporous WO₃ Gasochromic Films for Gas Sensing," *ACS Applied Nano Materials*, vol. 4, no. 8, pp. 8368-8375, 2021.
- [12] S. Hossain, W.-S. Chu, C. S. Lee, S.-H. Ahn, and D.-M. Chun, "Photocatalytic performance of few-layer Graphene/WO₃ thin films prepared by a nano-particle deposition system," *Materials Chemistry and Physics*, vol. 226, pp. 141-150, 2019.
- [13] L. Shen, G. Luo, J. Zheng, and C. Xu, "Effect of pH on the electrochromic and photoluminescent properties of Eu doped WO₃ film," *Electrochimica Acta*, vol. 278, pp. 263-270, 2018.
- [14] T. Ohishi, K. Ueguri, and K. Nakamura, "Low-Temperature Formation of a WO₃ Thin Film by the Sol-Gel Method Using Photo-Irradiation and Fabrication of a Flexible Hydrogen Sensor," *Materials Sciences and Applications*, vol. 12, no. 02, pp. 135, 2020.
- [15] R. Godbole, V. Godbole, P. Alegaonkar, and S. Bhagwat, "Effect of film thickness on gas sensing properties of sprayed WO₃ thin films," *New Journal of Chemistry*, vol. 41, no. 20, pp. 11807-11816, 2017.
- [16] B. Zhou, W. Feng, G. Gao, G. Wu, Y. Chen, and W. Li, "A low cost preparation of WO₃ nanospheres film with improved thermal stability of gasochromic and its application in smart windows," *Materials Research Express*, vol. 4, no. 11, pp. 115702, 2017.
- [17] W. Cheng, H. Ren, Y. Chen, D. Wu, S. Zhang, C. Yu, and F. Li, "Preparation of WO₃/Mo/CrNi/TiO₂ composite multifunctional photothermal conversion films with self-cleaning and low emissivity," *Frontiers in Energy Research*, pp. 1003, 2022.
- [18] Z. Wei, L. Xu, S. Peng, and Q. Zhou, "Application of WO₃ Hierarchical Structures for the Detection of Dissolved Gases in Transformer Oil: A Mini Review," *Front Chem*, vol. 8, pp. 188, 2020.
- [19] V. V. Ganbavle, S. V. Mohite, J. H. Kim, and K. Y. Rajpure, "Effect of solution concentration on physicochemical and gas sensing properties of sprayed WO₃ thin films," *Current Applied Physics*, vol. 15, no. 2, pp. 84-93, 2015.

- [20] S. S. Shendage, V. L. Patil, S. P. Patil, S. A. Vanalakar, J. L. Bhosale, J. H. Kim, and P. S. Patil, "NO₂ sensing properties of porous fibrous reticulated WO₃ thin films," *Journal of Analytical and Applied Pyrolysis*, vol. 125, pp. 9-16, 2017.
- [21] P. T. K. Shanmugasudram, M. Ramamurthy, "Growth and Characterization of Jet Nebulizer Spray Deposited n-type WO₃ thin films for Junction Diode Application," *Oriental Journal of Chemistry*, vol. Vol. 33 no. (5), pp. 2484-2491, 2017.
- [22] L. Sunasri, C. Luangchaisri, and T. Jutarosaga, "A study of WO_x films prepared by spray pyrolysis for electrochromic device," *Research Journal Phranakhon Rajabhat: Science and Technology*, vol. 13, no. 1, pp. 13-28, 2018.
- [23] K. Qiu, Q. Xie, D. Qiu, L. Cai, W. Wu, W. Lin, Z. Yao, B. Ai, Z. Liang, and H. Shen, "Power-loss analysis of a dopant-free ZnS/p-Si heterojunction solar cell with WO₃ as hole-selective contact," *Solar Energy*, vol. 165, pp. 35-42, 2018.
- [24] A. D. Thahir, A. J. Haider, and G. A. Ali, "Preparation of Nanostructure TiO₂ at Different Temperatures by Pulsed Laser Deposition as Solar Cell," *Engineering and Technology Journal*, vol. 34, no. 2 Part (A) Engineering, 2016.
- [25] Y.-C. Liang, and C.-W. Chang, "Preparation of orthorhombic WO₃ thin films and their crystal quality-dependent dye photodegradation ability," *Coatings*, vol. 9, no. 2, pp. 90, 2019.
- [26] G. Adilakshmi, A. S. Reddy, P. S. Reddy, and C. S. Reddy, "Electron beam evaporated nanostructure WO₃ films for gas sensor application," *Materials Science and Engineering: B*, vol. 273, pp. 115421, 2021.
- [27] T. Zhang, M. Paulose, R. Neupane, L. A. Schaffer, D. B. Rana, J. Su, L. Guo, and O. K. Varghese, "Nanoporous WO₃ films synthesized by tuning anodization conditions for photoelectrochemical water oxidation," *Solar Energy Materials and Solar Cells*, vol. 209, pp. 110472, 2020.
- [28] B. Au, K. Y. Chan, W. L. Pang, C. L. Lee, and A. H. Mustafa, "Tungsten oxide (WO₃) films prepared by sol-gel spin-coating technique." In *Solid State Phenomena*, vol. 280, pp. 71-75, 2018.
- [29] A. D. Faisal, R. A. Ismail, W. K. Khalef, E. T. Salim, et al., "Synthesis of ZnO nanorods on a silicon substrate via hydrothermal route for optoelectronic applications," *Optical and Quantum Electronics*, vol. 52, no. 4, pp. 1-12, 2020.
- [30] E. T. Salim, R. A. Ismail, and H. T. Halbos, "Deposition geometry effect on structural, morphological and optical properties of Nb₂O₅ nanostructure prepared by hydrothermal technique," *Applied Physics A*, vol. 126, no. 11, pp. 1-9, 2020.
- [31] K. H. Aboud, N. Jamal Imran, and S. M. H. Al-Jawad, "Structural, Optical and Morphological Properties Cadmium Sulfide Thin Films Prepared by Hydrothermal Method," *Journal of Applied Sciences and Nanotechnology*, vol. 1, no. 2, pp. 49-57, 2021.
- [32] A. Ani, P. Poornesh, A. Antony, I. V. Shchetinin, K. Nagaraja, S. Chattopadhyay, and K. Vinayakumar, "Impact of Ag on the Limit of Detection towards NH₃-Sensing in Spray-Coated WO₃ Thin-Films," *Sensors*, vol. 22, no. 5, pp. 2033, 2022.
- [33] J. H. K. V. V. Ganbavle, and K. Y. Rajpur, "Effect of Substrate Temperature on the Properties of Sprayed WO₃ Thin Films Using Peroxotungstic Acid and Ammonium Tungstate: A Comparative Study," *Journal of electronic materials*, vol. 44, no. 3, pp. 874-885, 2015.
- [34] M. Raja, J. Chandrasekaran, and M. Balaji, "The Structural, Optical and Electrical Properties of Spin Coated WO₃ Thin Films Using Organic Acid," *silicon*, vol. 9, no. 2, pp. 201-210, 2016.
- [35] M. Balaji, J. Chandrasekaran, and M. Raja, "Role of substrate temperature on MoO₃ thin films by the JNS pyrolysis technique for P-N junction diode application," *Materials Science in Semiconductor Processing*, vol. 43, pp. 104-113, 2016.
- [36] R. Shakoury, A. Arman, S. Rezaee, A. G. Korpi, S. Kulesza, C. Luna, M. Bramowicz, and M. Mardani, "Optical properties and morphology analysis of hexagonal WO₃ thin films obtained by electron beam evaporation," *Journal of Materials Science: Materials in Electronics*, vol. 32, no. 1, pp. 798-805, 2020.

- [37] V. V. G. S. V. Mohite, and K. Y. Rajpure, "Solar photoelectrocatalytic activities of rhodamine-B using sprayed WO₃ photoelectrode," *Journal of Alloys and Compounds*, vol. 655, pp. 106-113, 2016.
- [38] E. T. Salim, J. A. Saimon, M. K. Abood, M. A. Fakhri, et al., "Effect of silicon substrate type on Nb₂O₅/Si device performance: an answer depends on physical analysis," *Optical and Quantum Electronics*, vol. 52, no. 10, pp. 1-16, 2020.
- [39] I. Hadi, M. Jawad, and K. Hassoon, "Improvement of Substrates Properties by Incorporating Titanium Nanoparticles Deposited by DC Diode Sputtering Approach," *Journal of Applied Sciences and Nanotechnology*, vol. 2, no. 2, pp. 103-111, 2022.
- [40] M. Manickam, V. Ponnuswamy, C. Sankar, R. Suresh, et al., "Cobalt oxide thin films prepared by NSP technique: Impact of molar concentration on the structural, optical, morphological and electrical properties," *Optik*, vol. 127, no. 13, pp. 5278-5284, 2016.
- [41] R. David Prabu, S. Valanarasu, V. Ganesh, M. Shkir, et al., "Investigation of molar concentration effect on structural, optical, electrical, and photovoltaic properties of spray-coated Cu₂O thin films," *Surface and Interface Analysis*, vol. 50, no. 3, pp. 346-353, 2018.
- [42] M. Raja, J. Chandrasekaran, and M. Balaji, "Evaluation of microstructural and electrical properties of WO_{3-x} thin films for p-Si/n-WO_{3-x}/Ag junction diodes," *Optik*, vol. 127, no. 22, pp. 11009-11019, 2016.
- [43] I. Hasan, K. Khashan, and A. Hadi, "Study of the Effect of Laser Energy on the Structural and Optical Properties of TiO₂ NPs Prepared by PLAL Technique," *Journal of Applied Sciences and Nanotechnology*, vol. 2, no. 1, pp. 11-19, 2022.
- [44] R. Marnadu, J. Chandrasekaran, M. Raja, M. Balaji, et al., "Influence of metal work function and incorporation of Sr atom on WO₃ thin films for MIS and MIM structured SBDs," *Superlattices and Microstructures*, vol. 119, pp. 134-149, 2018.
- [45] V. V. Ganbavle, S. V. Mohite, G. L. Agawane, J. H. Kim, et al., "Nitrogen dioxide sensing properties of sprayed tungsten oxide thin film sensor: Effect of film thickness," *J Colloid Interface Sci*, vol. 451, pp. 245-54, Aug 1, 2015.
- [46] S. R. Bathe and P. S. Patil, "Electrochromic characteristics of fibrous reticulated WO₃ thin films prepared by pulsed spray pyrolysis technique," *Solar Energy Materials and Solar Cells*, vol. 91, no. 12, pp. 1097-1101, 2007.
- [47] S. Dabbous, T. Ben Nasrallah, J. Ouerfelli, K. Boubaker, et al., "Study of structural and optical properties of sprayed WO₃ thin films using enhanced characterization techniques along with the Boubaker Polynomials Expansion Scheme (BPES)," *Journal of Alloys and Compounds*, vol. 487, no. 1-2, pp. 286-292, 2009.
- [48] L. M. Bertus, A. Enesca, and A. Duta, "Influence of spray pyrolysis deposition parameters on the optoelectronic properties of WO₃ thin films," *Thin Solid Films*, vol. 520, no. 13, pp. 4282-4290, 2012.
- [49] F. Zahedi, R. Dariani, and S. Rozati, "Structural, optical and electrical properties of ZnO thin films prepared by spray pyrolysis: effect of precursor concentration," *Bulletin of Materials Science*, vol. 37, no. 3, pp. 433-439, 2014.
- [50] M. Baneto, A. Enesca, Y. Lare, K. Jondo, et al., "Effect of precursor concentration on structural, morphological and opto-electric properties of ZnO thin films prepared by spray pyrolysis," *Ceramics International*, vol. 40, no. 6, pp. 8397-8404, 2014.
- [51] V. V. Ganbavle, S. V. Mohite, J. H. Kim, K. Y. Rajpure, et al., "Effect of solution concentration on physicochemical and gas sensing properties of sprayed WO₃ thin films," *Current Applied Physics*, vol. 15, no. 2, pp. 84-93, 2015.
- [52] C. Das, J. Begum, T. Begum, S. Choudhury, et al., "Effect of thickness on the optical properties of GaAs thin films," *Journal of Bangladesh Academy of Sciences*, vol. 37, no. 1, pp. 83-91, 2013.

- [53] A. Abdelkrim, S. Rahmane, O. Abdelouahab, A. Hafida, et, al., "Effect of solution concentration on the structural, optical and electrical properties of SnO₂ thin films prepared by spray pyrolysis," *Chinese Physics B*, vol. 25, no. 4, p. 046801, 2016.
- [54] M. Saleem, M. Al-Kuhaili, S. Durrani, A. Hendi, et, al., "Influence of hydrogen annealing on the optoelectronic properties of WO₃ thin films," *International journal of hydrogen energy*, vol. 40, no. 36, pp. 12343-12351, 2015.
- [55] K. Patel, C. Panchal, V. Kheraj, M. Desai, et, al., "Growth, structural, electrical and optical properties of the thermally evaporated tungsten trioxide (WO₃) thin films," *Materials Chemistry and Physics*, vol. 114, no. 1, p. 475-478, 2009.
- [56] J. C. M. Raja, M. Balaji, and B. Janarthanan, "Impact of annealing treatment on structural and dc electrical properties of spin coated tungsten trioxide thin films for Si / WO₃ / Ag junction diode," *Materials Science in Semiconductor Processing*, vol. 56 pp. 145–154, 2016.
- [57] R. Mukherjee, C. S. Prajapati, and P. P. Sahay, "Tailoring the Microstructural, Optical, and Electrical Properties of Nanocrystalline WO₃ Thin Films Using Al Doping," *Journal of Materials Engineering and Performance*, vol. 23, no. 9, p. 3141-3151, 2014.
- [58] F. Urbach, "The long-wavelength edge of photographic sensitivity and of the electronic absorption of solids," *Physical Review*, vol. 92, no. 5, p. 1324, 1953.
- [59] M. Saleem, "Effect of zinc acetate concentration on the structural and optical properties of ZnO thin films deposited by Sol-Gel method," *International Journal of the Physical Sciences*, vol. 7, no. 23, 2012.
- [60] R. Marnadu, J. Chandrasekaran, S. Maruthamuthu, V. Balasubramani, P. Vivek, and R. Suresh, "Ultra-high photoresponse with superiorly sensitive metal-insulator-semiconductor (MIS) structured diodes for UV photodetector application," *Applied Surface Science*, vol. 480, pp. 308-322, 2019.
- [61] R. S. Vemuri, K. K. Bharathi, S. K. Gullapalli, C. V. Ramana, et, al., "Effect of structure and size on the electrical properties of nanocrystalline WO₃ films," *ACS Appl Mater Interfaces*, vol. 2, no. 9, p. 2623-8, 2010.
- [62] H. Attouche, S. Rahmane, S. Hettal, N. Kouidri, et, al., "Precursor nature and molarities effect on the optical, structural, morphological, and electrical properties of TiO₂ thin films deposited by spray pyrolysis," *Optik*, vol. 203, p. 163985, 2020.
- [63] R. E. I. Schropp, and A. Madan, "Properties of conductive zinc oxide films for transparent electrode applications prepared by rf magnetron sputtering," *Journal of Applied Physics*, vol. 66, no. 5, pp. 2027-2031, 1989.